Communications in Applied and Industrial Mathematics,
ISSN 2038-0909, e-533

DOI: 10.1685/journal.caim.533
Research Paper

A non-local KdV-Burgers equation: Numerical study of travelling waves

Carlota M. Cuesta

University of the Basque Country (UPV/EHU),
Faculty of Science and Technology, Department of Mathematics,
Aptdo. 644, 48080 Bilbao, Spain.
E-mail: carlotamaria.cuesta@ehu.es

Dedicated to Professor Francesco Mainardi
on the occasion of his retirement

Communicated by Gianni Pagnini and Enrico Scalas

Abstract

We present numerical simulations that support our previous study of travelling wave solutions of a Korteweg-de Vries-Burgers equation with a non-local diffusion term [1]. This model equation arises in the analysis of a shallow water flow by performing formal asymptotic expansions associated to the triple-deck regularisation (which is an extension of classical boundary layer theory). The resulting non-local operator is of the fractional derivative type with order between 1 and 2. Travelling wave solutions are typically analysed in relation to shock formation in the full shallow water problem. In this paper we give numerical evidence of stability of non-monotone travelling wave. We also confirm the existence of travelling waves that are everywhere monotone except over a bounded interval where they exhibit oscillations.

Keywords: `non-local evolution equation, KdV-Burgers equation, fractional derivative, travelling waves.`

AMS subject classification: `47J35, 26A33, 35C07`

1. Introduction.

In this note we present numerical solutions in order to study the travelling wave problem associated to the following Cauchy problem:

$$\partial_t u + \partial_x u^2 = \partial_x \mathcal{D}^\alpha u + \tau \partial_x^3 u\,, \quad x \in \mathbb{R}\,,\ t \geq 0\,, \tag{1}$$

$$u(x,0) = u_0(x)\,, \quad x \in \mathbb{R}\,, \tag{2}$$

Received on 01 31, 2014. Accepted on 10 06, 2014. Published on 08 10, 2015.

with $\tau > 0$ and $0 < \alpha < 1$, where $\mathcal{D}^\alpha$, that acts on the spatial variable x, denotes the following non-local operator (here applied to an arbitrary function $f(x)$),

$$\mathcal{D}^\alpha f(x) = d_\alpha \int_{-\infty}^{x} \frac{f'(y)}{(x-y)^\alpha} dy\,, \text{ with } d_\alpha = \frac{1}{\Gamma(1-\alpha)} > 0\,, \tag{3}$$

Γ being the Gamma function. This can be viewed as a Fractional Caputo derivative of order α (see e.g. [2]), thus the non-local operator $\partial_x \mathcal{D}^\alpha$ in (1) has order $1+\alpha \in (1,2)$.

We are interested, in particular, in analysing the behaviour and dynamic stability of travelling wave solutions. These are solutions of the form $u(x,t) = \phi(\xi)$ where $\xi = x - ct$, for some constant wave speed c, and that approach constant values as ξ tends to ∞ and to $-\infty$. More precisely, if ϕ depends on x and t only through the travelling wave variable ξ, then $\mathcal{D}^\alpha \phi$ does too, and $\phi(\xi)$ must satisfy

$$-c\phi' + (\phi^2)' = (\mathcal{D}^\alpha \phi)' + \tau \phi'''\,, \quad ' = \frac{d}{d\xi}\,.$$

This equation can be integrated once, to obtain

$$h(\phi) = \mathcal{D}^\alpha \phi + \tau \phi''\,, \quad h(\phi) := -c(\phi - \phi_-) + \phi^2 - \phi_-^2\,, \tag{4}$$

where

$$\lim_{\xi \to -\infty} \phi(\xi) = \phi_-\,, \quad \lim_{\xi \to \infty} \phi(\xi) = \phi_+\,, \tag{5}$$

and

$$c = \phi_+ + \phi_-\,. \tag{6}$$

Here (6) is the so-called Rankine-Hugoniot condition and is obtained by applying (5) to (4). We shall further assume that the entropy condition

$$\phi_- > \phi_+\,, \tag{7}$$

is satisfied.

The travelling wave problem (4)-(5) has been studied rigorously in [1]. Our aim in this paper is to contrast our rigorous results and conjectures with numerical examples. In order to do that we present a numerical algorithm that solves (4)-(5), and another that approximates (1)-(2) with an initial condition that satisfies the same far-field behaviour as a travelling wave solution, i.e. with $u_0(x)$ such that $\lim_{x\to-\infty} u_0(x) = \phi_-$ and $\lim_{x\to\infty} u_0 = \phi_+$.

DOI: 10.1685/journal.caim.533

The algorithms presented here are simple but good enough to approximate these problems; they serve as an auxiliary tool to illustrate the behaviour of the solutions.

In [3] travelling waves for (1) with $\tau = 0$ were analysed. In this case travelling waves are monotone, as it is the case for the classical (or local) Burgers equation. In [1] we analyse rigorously (1) with $\tau > 0$. We prove the existence of travelling waves for all values of τ and show dynamic stability of travelling waves provided that they are monotone. The analysis guarantees the monotonicity of the waves for small values of the parameter τ. We do not have a quantification of the critical τ for which the transition from monotone to oscillatory behaviour occurs, however.

In this paper we aim to complement our previous rigorous mathematical study with numerical examples. In particular, the examples presented here show that there are monotone travelling waves for values of τ that are not necessarily too small. They also suggest that non-monotone travelling waves are stable for moderate and large values of τ.

We remark that equation (1) with $\alpha = 1/3$ and either a quadratic flux, as above, or a cubic one, has been derived from a model of two layer shallow water flow by performing formal asymptotic expansions associated to the triple-deck (boundary-layer) theory (see, e.g. [4] and [5]). Travelling wave solutions in this model resemble the inner structure of small amplitude shock waves for the original shallow water problem. We point out that there are other models where such fractional derivative terms arise similarly, see, for instance [6], [7], [8], [9] and [10].

The paper is organised as follows. In Section 2 a summary of the derivation of (1) is presented. In Section 3 we briefly revise the results of [1]. Section 4 is dedicated to the description and the analysis of the numerical schemes. The numerical examples are shown in Section 5.

2. Motivation of the model.

In this section we aim to summarise the derivation of (1). We refer to [5] where this derivation is performed in detail.

The situation described in [5] is a two-layered (stratified) shallow water flow over a solid surface with small viscosity. The motion is thus governed by the incompressible form of the Navier-Stokes equations in a limit where the characteristic horizontal length-scale is very large compared to the characteristic height of the fluid and where viscosity terms are small compared to convective ones in the majority of the flow-field. The leading order term of this limit case results in a system of nonlinear hyperbolic partial differential

equations of the form

$$\frac{\partial \mathbf{z}}{\partial t} + A(\mathbf{z})\frac{\partial \mathbf{z}}{\partial x} = 0 \tag{8}$$

where $\mathbf{z}$ is the vector of four unknowns (in this case the thickness of each layer of fluid and the horizontal fluxes) and $A(\mathbf{z})$ is a non-jacobian matrix. As a further simplification one performs a perturbation around a constant solution $\mathbf{z_0}$ such that $\det(A(\mathbf{z_0})) = 0$. This gives to leading order the linear behaviour

$$\frac{\partial \mathbf{z_1}}{\partial t} + A(\mathbf{z_0})\frac{\partial \mathbf{z_1}}{\partial x} = 0\,,$$

which for large times reduces to

$$A(\mathbf{z_0})\mathbf{z_1} = 0\,.$$

Thus there exists a scalar function $P(x,t)$ such that $\mathbf{z_1}(x,t) = P(x,t)\mathbf{r}$, where $\mathbf{r}$ is a (non-trivial) right eigenvector of $A(\mathbf{z_0})$. Considering higher order terms gives a solvability condition of the form

$$\frac{\partial P}{\partial t} + \frac{\partial F(P)}{\partial x} = 0$$

where $F(P)$ is either a quadratic polynomial or a cubic one, depending on the initial and boundary conditions.

It is well-known that hyperbolic systems, such as (8), may exhibit solutions that develop discontinuities or shock waves (see e.g. [11]). These shock waves correspond to the so called hydraulic-jumps or bores in the present context. In order to investigate the internal structure of shock waves is customary to consider the viscosity of the system or introduce it artificially. The above approximation neglects viscosity terms coming from the full Navier-Stokes model. These terms become important near the bottom boundary, however, and therefore a boundary layer needs to be introduced. The model above also lacks the effect due to the stream curvature that becomes important near shock waves.

In [4] (for the single layer case) and in [5] (see also [12]) the authors keep track of the viscosity on the bottom boundary in a way consistent with the Navier-Stokes equations, by means of matched asymptotic expansions in the limit of the Reynolds number tending to infinity. As a consequence a distinguished limit associated with a *triple deck* problem is presented[a].

[a] We recall that the main idea of the of triple deck theory (see e.g. [13]) is that the leading order outer flow is not independent of the boundary layer flow, unlike in the classical Prandtls theory [14].

DOI: 10.1685/journal.caim.533

These considerations lead to a system of the type (8) with the solvability condition, written in the inner variables,

$$F(P) = a_1 P^3 + a_2 P^2 + a_3 P\,, \tag{9}$$

$$\frac{\partial P}{\partial T} + \frac{\partial}{\partial X} F(P) = C_1 \frac{\partial^3 P}{\partial X^3} + C_2 \frac{\partial B}{\partial X}\,, \tag{10}$$

for some constants a_i $(i = 1, 2, 3)$ and C_j $(j = 1, 2)$, and where B is a function determined by the displacement in the inner flow. The third order term results from adding the effect of the stream curvature.

In the inner flow (main deck) the equations are similar to the classical boundary layer ones and B appears as part of the matching conditions. The weak interaction limit, where the influence of the displacement is small, gives a simpler situation where the equations in the boundary layer can be linearised and to leading order one gets

$$B(X,T) = C d_\alpha \int_\infty^X \frac{\partial_Z P(Z,T)}{(X-Z)^{1/3}}\, dZ\,,$$

for some constant C. This expression coupled with (9)-(10) yields a equation of the type (1).

3. Summary of known rigorous results.

We start by recalling some basic properties of the operator $\mathcal{D}^\alpha$. Applied to a function $f(x)$, it can be written as the convolution of $f'(x)$ with $\theta(x)x^{-\alpha}/\Gamma(1-\alpha)$, where θ is the Heaviside function. One can write the integral operator (3) as follows

$$(\mathcal{D}^\alpha f)(x) = d_\alpha \int_{-\infty}^{x_0} \frac{f'(y)}{(x-y)^\alpha} dy + d_\alpha \int_{x_0}^{x} \frac{f'(y)}{(x-y)^\alpha} dy\,, \text{ for some } x_0 < x\,,$$

and treat the first term as a known function, whereas the second one is a left-sided Caputo derivative, that we denote by $\mathcal{D}^\alpha_{x_0}$, indicating that the integration is from a finite value x_0, i.e.

$$\mathcal{D}^\alpha_{x_0} f(x) := d_\alpha \int_{x_0}^{x} \frac{f'(y)}{(x-y)^\alpha}\, dy\,.$$

In [1] we prove the existence of (4)-(5). The proof follows three steps. First, we show 'local' existence. This is based on linearisation about $\phi = \phi_-$, this reads

$$h'(\phi_-)V = \mathcal{D}^\alpha V + \tau V''\,, \tag{11}$$

and has solutions of the form $V(\xi) = be^{\lambda\xi}$, $b \in \mathbb{R}$, where $\lambda > 0$ is the unique positive real solution of

$$\tau z^2 + z^\alpha - h'(\phi_-) = 0 \tag{12}$$

(see [1]). We prove that these are the only solutions that decay to 0 as $\xi \to -\infty$ in some suitable regular weighted spaces. The linearisation in particular gives that there are solutions that decrease from the value ϕ_- in some interval $(-\infty, \bar{\xi})$ for a negative enough $\bar{\xi}$.

Also it is not difficult to deduce the asymptotic behaviours of the positive real root, λ, in particular, we shall need later that

$$\lambda = \frac{\sqrt{h'(\phi_-)}}{\tau^{\frac{1}{2}}} - \frac{h'(\phi_-)^{\alpha-1}}{\tau^{\frac{1+\alpha}{2}}} + O(\tau^{-\gamma}) \quad \text{as} \quad \tau \to +\infty \tag{13}$$

where $\gamma > (1+\alpha)/2$ depends on α.

The next step in the proof is to show that the solution constructed *near* $-\infty$ can be extended with the same regularity to $\mathbb{R}$. This step allows to show that if a travelling wave solution tends to a constant value as $\xi \to \infty$ then that constant must be ϕ_+. In the final step, we show that, indeed, the solutions of (4) satisfying $\lim_{\xi\to-\infty} \phi(\xi) = \phi_-$ tend to a constant as $\xi \to \infty$.

The existence proof does not give much information on the monotonicity of the travelling wave solutions. This is a non-trivial issue for general solutions. We know that if $\tau = 0$ (see [3]) the travelling waves are monotone decreasing. In the classical KdV-Burgers case (with $\partial_x^2 u$ in place of $\partial_x \mathcal{D}^\alpha$ in (1)), it is easy to see that the waves are monotone if $\tau \leq -1/(4h'(\phi_+))$ (see [15]). In fact, travelling waves are heteroclinic connections of the corresponding system of Ordinary Differential Equations and can be analysed by standard techniques.

We expect a similar behaviour for (4), although the decay of ϕ towards ϕ_+ is not exponential, as we clarify below. It is, however, hard to quantify the value of τ for which there is a transition from monotone to oscillatory waves. We can, nevertheless, prove two things:

First, we are able to show that monotonicity holds for τ small enough in an interval $(-\infty, \xi_\tau)$ where $\xi_\tau = O(\tau^{-1/(2-\alpha)})$ as $\tau \to 0$. In the proof we use a variation of constant formulation, that can be found in [16], of the equation (4) *linearised* about ϕ_-.

Finally, in [1] we can show that in the right tail (i.e. for an interval of the form $(\xi_\delta, \infty]$ for a large enough ξ_δ so that ϕ is very close to ϕ_+) travelling wave solutions are monotone as long as τ is small enough. This does not imply that the waves are decreasing in the whole of the domain, however. The idea is to use again the variation of constant formulation for,

DOI: 10.1685/journal.caim.533

essentially, (4) linearised about ϕ_+. This gives and expression for $\phi - \phi_+$ of the form

$$\phi(\xi)-\phi_+ = (\phi(\xi_\delta)-\phi_+)v(\xi-\xi_\delta)+\frac{\tau}{h'(\phi_+)}\phi(\xi_\delta)'v'(\xi-\xi_\delta)+R(\phi,\xi,\xi_\delta)\,, \tag{14}$$

where the last term $R(\phi, \xi, \xi_\delta)$ tends to 0 as $\xi \to \infty$ at the same rate as either $|\phi(\xi) - \phi_+|^2$ or $|\phi(\xi) - \phi_+|/\xi^\alpha$ does. More importantly, the function $v(\zeta)$ reads

$$v(\zeta) = -h'(\phi_+)\frac{\sin(\alpha\pi)}{\pi}\int_0^\infty e^{-\zeta r}K_\alpha(r)\,dr + 2\mathrm{Re}\left(e^{s_1\zeta}\frac{\tau s_1 + s_1^{\alpha-1}}{2\tau s_1 + \alpha s_1^{\alpha-1}}\right)\,,$$

where s_1 is the solution of $\tau z^2 + z^\alpha - h'(\phi_+) = 0$ with positive imaginary part (see [1]), and $\beta = \arg(s_1) \in (\pi/2, \pi)$. An asymptotic expansion of s_1 as $\tau \to 0^+$ reads

$$s_1 = e^{i\frac{\pi}{2-\alpha}}\tau^{-\frac{1}{2-\alpha}} + O(1) \quad \text{as} \quad \tau \to 0^+. \tag{15}$$

Moreover, the function K_α has the property, see [16], that

$$\int_0^\infty e^{-\zeta r}K_\alpha(r)dr \sim \frac{\Gamma(\alpha)}{a^2}\frac{1}{\zeta^\alpha} + O\left(\frac{1}{\zeta^{\alpha+2}}\right) \quad \text{as} \quad \zeta \to \infty\,, \tag{16}$$

with $a = h'(\phi_+)$. The non-monotone contributions for large ζ are thus given by the exponential oscillatory term of $v(\zeta)$. Observe that $\mathrm{Re}\left(e^{s_1\zeta}\frac{\tau s_1+s_1^{\alpha-1}}{2\tau s_1+\alpha s_1^{\alpha-1}}\right)$ has infinitely many oscillations with frequency $\omega = \rho\sin\beta = \mathrm{Im}(s_1)$, but its amplitude decreases exponentially like $e^{(|s_1|\cos\beta)\zeta}$ as $\zeta \to \infty$ (because of (15) and $\cos(\beta) < 0$). Thus taking ξ large enough and τ small enough the small oscillations get damped by the algebraic decaying term (16) of the monotone part.

On the other hand, the real part of s_1 tends to 0 as $\tau \to \infty$ and its imaginary part tends to infinity. This suggests that oscillations persist for much larger intervals of ξ if τ is very large than if τ is small. This analysis in the tail does not apply to the behaviour of ϕ where its value is not close to either of the far field values. There ϕ might or might not be oscillatory. In this regard, we notice that the scaling $t = \tau^{1/2}t'$ and $x = \tau^{1/2}x'$ applied to (1) gives the rescaled equation

$$\partial_{t'}u + \partial_{x'}u^2 = \tau^{-\alpha/2}\partial_{x'}\mathcal{D}^\alpha u + \partial^3_{x'}u\,.$$

If $\alpha = 1$ the limit $\tau \to \infty$ is not uniform (e.g. [17]) and it is well-know that solutions become highly oscillatory, i.e. in the limit to the KdV equation. Such behaviour is to be expected here as well.

The numerical results below, show that travelling wave solutions are monotone for small and moderate values of τ. They also show that oscillations may appear away from the tails. And that for large values of τ oscillations of large amplitude persist beyond the right tail.

In [1] we can also prove the dynamic stability of monotone travelling wave solutions, is the following sense. If ϕ is a monotone travelling wave and $u_0(x)$ is close enough to a travelling wave solution in a suitable sense, then there exists a unique global solution, with initial condition $u_0(x)$, that approaches a travelling wave solution. The proof by integral estimates relies on the monotonicity of the waves. The numerical examples presented here suggest that stability of the non-monotone waves also holds.

4. Numerical Schemes.

In this section we briefly describe the numerical methods performed in order to approximate both the travelling wave equation (4) and the initial value problem for (1) on $\mathbb{R}$. The methods are simple, but good enough to illustrate the behaviour of the solutions we look for. We show pertinent convergence tables below. The numerical simulations are carried out with MATLAB.

4.1. *A shooting method for (4).*

We compute (4) by the Heun's method (a second order explicit Runge-Kutta method, see e.g. [18]) leaving the integral and nonlinear terms as given from the previous steps. Here we do not consider Runge-Kutta methods applied to (non-linear) integral operators as in e.g. [19]. The integral term is first integrated by parts and we use the trapezoidal rule to approximate the resulting integral. The convergence and order of the full discretisation is analysed below with Table 1. We first describe the discretisation in detail.

We start the iteration at a sufficiently negative value of ξ, ξ_0, with ϕ given by an exponential initial condition with exponent λ. Since this equation is of second order, it is convenient to write it as a system of two first order equations:

$$\begin{aligned} \phi' &= \psi\,, \\ \tau\psi' &= h(\phi) - d_\alpha \int_{-\infty}^{\xi} \frac{\psi(y)}{(\xi - y)^\alpha}\, dy\,. \end{aligned} \tag{17}$$

Due to the singular character of the integral term $\mathcal{D}^\alpha\phi(\xi)$ around ξ, we seek to remove the singularity by using the far-field behaviour and by integrating

DOI: 10.1685/journal.caim.533

by parts this operator. The result is an integral operator with a non-singular kernel:

$$\int_{-\infty}^{\xi} \frac{\psi(y)}{(\xi-y)^{\alpha}} dy = \frac{1}{1-\alpha} \int_{-\infty}^{\xi} \psi'(y)(\xi-y)^{1-\alpha} dy + \frac{1}{1-\alpha} \left(- \lim_{y\to\xi} \psi(y)(\xi-y)^{1-\alpha} + \lim_{y\to-\infty} \psi(y)(\xi-y)^{1-\alpha} \right). \tag{18}$$

The first term on the left-hand side of (18) vanishes due to the regularity of ϕ in ξ (see [1]). The second term is also zero, as one can check by using the far-field behaviour (5) and the fact that we only consider solutions that grow exponentially from $-\infty$. We shall keep this term at the point where the domain is truncated ξ_0, i.e. at the initial step of the numerical integration. The price to pay by removing the singularity in this way is that we must approximate the derivative of ψ in every step of the integration. We do this by a second order finite difference approximation.

For completeness, we write the scheme that solves the initial value problem for (17)-(18). We let $\Delta\xi$ denote the integration step size and (ϕ^n, ψ^n) denote the solution at $\xi_n = \xi_0 + n\Delta\xi$. The solution at ξ_{n+1}, is then computed by means of

$$\phi^{n+1} = \phi^n + \frac{\Delta\xi}{2}(k_{1,\phi} + k_{2,\phi}),$$
$$\psi^{n+1} = \psi^n + \frac{\Delta\xi}{2}(k_{1,\psi} + k_{2,\psi}),$$

with

$$k_{1,\phi} = \psi^n,$$
$$k_{1,\psi} = \frac{1}{\tau}\left(-\mathcal{D}^{\alpha}_{\Delta\xi}\psi^n + h(\phi^n)\right),$$
$$k_{2,\phi} = \psi^n + (\Delta\xi)\, k_{1,\psi},$$
$$k_{2,\psi} = \frac{1}{\tau}\left(-\mathcal{D}^{\alpha}_{\Delta\xi}(\psi^n + \Delta\xi\, k_{1,\psi}) + h(\phi^n + (\Delta\xi)\, k_{1,\phi})\right)$$

where the discrete operator $\mathcal{D}^{\alpha}_{\Delta\xi}$ represents the discretisation of $\mathcal{D}^{\alpha}_{\xi_0}$. In order to obtain this discretised operator we use (18) and a simple trapezoidal rule to compute the integral: If we denote by $D_{\Delta\xi}$ the discrete derivative by central differences, $D_{\Delta\xi}\psi^k = (\psi^{k+1} - \psi^{k-1})/(2\Delta\xi)$ for $k = 1, \ldots, n-1$ and with $D_{\Delta\xi}\psi^0 = \frac{-3\psi^0+4\psi^1-\psi^2}{2\Delta\xi}$ and $D_{\Delta\xi}\psi^n = \frac{3\psi^n-4\psi^{n-1}+\psi^{n-2}}{2\Delta\xi}$ at the end

points ξ_0 and ξ_n, we have

$$D^{\alpha}_{\Delta\xi}\psi^n = \frac{h}{2}\frac{1}{\Gamma(2-\alpha)}\sum_{k=0}^{n-1}\left(D_{\Delta\xi}\psi^k(\xi_n-\xi_k)^{1-\alpha} + D_{\Delta\xi}\psi^{k+1}(\xi_n-\xi_{k+1})^{1-\alpha}\right) + \frac{1}{\Gamma(2-\alpha)}\psi^0(\xi_n-\xi_0)^{1-\alpha}.$$

We observe that we have to impose the initial condition at ξ_0, ξ_1 and ξ_2 in order to compute the integral term. We shall just impose that $\phi^k = \phi_- - e^{\lambda\xi_k}$ and $\psi^k = -\lambda e^{\lambda\xi_k}$ for $k = 0, 1, 2$, where λ is the real positive solution of (12) (this is approximated by using the MATLAB package fsolve).

The convergence of the method is shown in Table 1. On the one hand, we compute the error in the discrete L^∞-norm between a numerical solution computed for a $\Delta\xi$ and the one computed with $\Delta\xi/2$, we repeat this computation for the solution computed with $\Delta\xi/2$ and the one computed with $\Delta\xi/4$ and so on. This shows the convergence (as a Cauchy sequence) of the method. We also obseve that the order of the method is just above 1, because the error diminishes more than half when $\Delta\xi$ is halved, except for a small oscillation. To verify this we also compute the error between solutions and the one computed for a very fine grid (here $\Delta\xi = 1/2^{11}$).

Table 1. In this table, for a given value of $\Delta\xi$, $\phi(\Delta\xi)$ denotes the numerical solution of (17)-(18) with $\tau = 1$ and $\alpha = 1/3$ on the interval $[-32, 1000]$.

$\Delta\xi$	$\|\phi(\Delta\xi) - \phi(\Delta\xi/2)\|_\infty$	$\|\phi(\Delta\xi) - \phi(1/2^{11})\|_\infty$
1	$2.9269 \cdot 10^{-2}$	$2.7596 \cdot 10^{-2}$
$1/2$	$5.8483 \cdot 10^{-3}$	$9.5589 \cdot 10^{-3}$
$1/2^2$	$2.8062 \cdot 10^{-3}$	$3.7106 \cdot 10^{-3}$
$1/2^3$	$1.3135 \cdot 10^{-3}$	$1.3230 \cdot 10^{-3}$
$1/2^4$	$3.1652 \cdot 10^{-4}$	$6.6481 \cdot 10^{-4}$
$1/2^5$	$1.8639 \cdot 10^{-4}$	$8.2030 \cdot 10^{-4}$
$1/2^6$	$2.3164 \cdot 10^{-4}$	$6.4193 \cdot 10^{-4}$
$1/2^7$	$1.8091 \cdot 10^{-4}$	$4.1065 \cdot 10^{-4}$
$1/2^8$	$1.1854 \cdot 10^{-4}$	$2.2978 \cdot 10^{-4}$
$1/2^9$	$7.0976 \cdot 10^{-5}$	$1.1125 \cdot 10^{-4}$
$1/2^{10}$	$4.0275 \cdot 10^{-5}$	$4.0275 \cdot 10^{-5}$

4.2. *A finite difference scheme for (1).*

We now briefly discuss the numerical method employed to compute the evolution problem. Since we want to give evidence of stability of non-monotone travelling waves we shall take as initial condition a smooth one

DOI: 10.1685/journal.caim.533

that satisfies the far-field behaviour. A function that exemplifies these requirements is, for instance,

$$u_0(x) = \frac{1}{2}\left(\phi_+ + \phi_- - (\phi_- - \phi_+)\tanh(x)\right) . \tag{19}$$

We truncate the domain $\mathbb{R}$ and consider the problem on a closed interval $[-R, L]$ for some R, $L > 0$ large enough and generally with $L \geq R$. We take a uniform partition of this interval, let its nodes be denoted by $x_0 = -R, \ldots, x_N = L$, and, as above, we let $\Delta x = (R+L)/N$ denote the spatial step size. We let Δt be the temporal step size and denote by $t_k = k\Delta t$ for all $k = 0, 1, \ldots$ the temporal step. We shall write u_i^k for the value of the solution of the discretised problem at the point (x_i, t_k).

As we do in (18) for the travelling wave problem, we integrate by parts the integral operator. In this case we assume that the far-field behaviour satisfied by the initial condition is conserved by the solution and that $\partial_x u(x,t)$ tends to zero at a faster rate than $|x|^{\alpha-1}$ as $x \to -\infty$. The integration by parts then gives

$$d_\alpha \int_{-\infty}^{x} \frac{\partial_x u(y,t)}{(x-y)^\alpha} dy = \frac{1}{\Gamma(2-\alpha)} \int_{-\infty}^{x} \partial_x^2 u(y,t)(x-y)^{1-\alpha} dy \, . \tag{20}$$

The numerical discretisation is thus for (1) with the non-local term

$$\partial_x \mathcal{D}^\alpha u(x,t) = \frac{1}{\Gamma(2-\alpha)} \partial_x \left(\int_{-\infty}^{x} \partial_x^2 u(y,t)(x-y)^{1-\alpha} dy \right) .$$

We discretised (1) in time by the backward (implicit) Euler scheme, except for the non-linear term that is treated explicitly. We perform a finite differences scheme in the space variable. The latter is done by generating four matrices that approximate the linear operators of the equation. First, we generate the fourth order differentiation matrices that approximate the first, second and third derivative operators, which we let be denoted by D_1, D_2 and D_3. The central diagonals of the matrices are obtained from the finite differences approximations (we skip here the dependency on k for simplicity of notation):

$$\begin{aligned}
\partial_x u_i &\sim \frac{u_{i-2} - 8u_{i-1} + 8u_{i+1} - u_{i+2}}{12\Delta x} \\
\partial_x^2 u_i &\sim \frac{-u_{i-2} + 16u_{i-1} - 30u_i + 16u_{i+1} - u_{i+2}}{12(\Delta x)^2} \\
\partial_x^3 u_i &\sim \frac{-u_{i-2} + 2u_{i-1} - 2u_{i+1} + u_{i+2}}{2(\Delta x)^3},
\end{aligned}$$

and we add in each case the corresponding one side approximation in the first two and last two rows of the matrix (see e.g [20]).

The fourth matrix we generate is one that approximates the operator (20), or equivalently, the convolution operator

$$\frac{1}{\Gamma(2-\alpha)}\int_{-\infty}^{\infty}\partial_x^2 u(y,t)K(x,y)dy\,,\quad K(x,y):=(x-y)^{1-\alpha}\theta(x-y)\,, \tag{21}$$

where θ is the Heaviside function.

We shall denote by D_α the discretisation of (21) and we generate it as follows. We use that integrating is the inverse operation of differentiating, thus we seek to invert D_1 in order to obtain the integration operator. Since the value of the integral is 0 at x_0, we fix this constant of integration by suppressing the first column of D_1, we denote the resulting matrix by $\tilde{D}_1$, and then we compute the pseudo-inverse (see e.g. [21]) of $\tilde{D}_1$, which in this case is $\tilde{I}=(\tilde{D}_1^T\tilde{D}_1)^{-1}\tilde{D}_1^T$. Finally, adding a first column of zeros to $\tilde{I}$ we obtain a square matrix I with the zero entries at the positions of x_0. The final step is to create the convolution-by-K operator. In order to do that we multiply every m-th row of I up to the m-th element by the vector $K(x_m,y_i)$ with $i=0,\dots,m$ and the rest by 0. This gives the discrete approximation of (21), D_α.

We test the correctness of the discretisation of $\partial_x\mathcal{D}^\alpha$ that, in our notation, is the discrete operator D_1D_α. For doing that we choose to apply it to e^x, since we know that $\mathcal{D}^\alpha e^x=e^x$. For this test we take $x\in[-10,20]$, which is a relatively large domain since the value of the exponential at $x=20$ is rather large; $e^{20}\approx 4.85\cdot 10^8$. In Table 2 we compute the relative error $\|D_1D_\alpha e^x-e^x\|_{L^\infty}/\|e^x\|_{L^\infty}$ for different values of Δx. The errors for this example are good enough for our purposes, taking into account that the solutions of the full equation are uniformly bounded and the function we are testing with is not.

Table 2. Relative error $\|D_1D_\alpha e^x-e^x\|_{L^\infty}/\|e^x\|_{L^\infty}$ with $\alpha=1/3$ on the interval $[-10,20]$ for different values of Δx.

Δx	1	1/2	1/4	1/8	1/16
Rel. err.	0.1070	0.0671	0.0545	0.0404	0.0275

Summarising, in the discrete operator notation the scheme reads

$$(Id-D_1D_\alpha-\tau D_3)^{-1}u^{k+1}=u^k-2\,\Delta t\,u^kD_1u^k\,,$$

where Id represents the identity matrix. This system must be supplemented with boundary conditions. In the examples below, we fixed the left boundary condition to $u(-R,t)=\phi_-$ and apply zero Neumann on the right boundary.

DOI: 10.1685/journal.caim.533

We end this section by testing the discretisation of (1)-(2). We are using a finite difference scheme, and as long as the solutions of the original problem are smooth (which they are for smooth initial data, see [1]) the convergence of the method is guaranteed by application of Taylor's theorem. On the other hand, the method reveals itself as highly stable. In fact, with Δt as large as 0.1 we are able to advance up to a $t = 1000$ irrespectively of the considered Δx. More precisely, we have tested the stability by taking into account that the solutions of (1) have uniformly bounded solutions for uniformly bounded initial data (again, see [1]). For all the experiments that we have performed, the maximal Δt (for values of $\Delta x = 2, 1, 1/2, \dots$) that gives uniformly bounded solutions is around 0.15 for up to $t = 2000$.

In order to get an idea of the convergence and order of the method we include two tables of errors. First, in Table 3 for fixed values of t and of Δx we evaluate the error (in the discrete L^∞-norm) between the solution for a given Δt and the solution for $\Delta t/2$, then for the difference between the solution for $\Delta t/2$ and the solution for $\Delta t/4$, and so on. This same test is repeated fixing several values of Δx. The table shows that the error diminishes more than half the amount if we half Δt,indicating a convergence order of just above one. The errors also decrease for decreasing Δx, showing faster convergence for smaller Δx's.

Table 3. For a fixed value of Δx we compute the numerical solution at $t = 100$ for different values of Δt. Let $u_{\Delta x}(\Delta t, t = 100)$ denote such numerical solution. Then, in every column the table shows the error $\|u_{\Delta x}(\Delta t, t = 100) - u_{\Delta x}(\Delta t/2, t = 100))\|_\infty$.

Δt	$\Delta x = 1$	$\Delta x = 1/2$	$\Delta x = 1/4$	$\Delta x = 1/8$	$\Delta x = 1/16$
1/10	$8.6622 \cdot 10^{-3}$	$8.5277 \cdot 10^{-3}$	$8.3173 \cdot 10^{-3}$	$8.2690 \cdot 10^{-3}$	$8.2493 \cdot 10^{-3}$
1/20	$3.7666 \cdot 10^{-3}$	$3.6431 \cdot 10^{-3}$	$3.5871 \cdot 10^{-3}$	$3.5685 \cdot 10^{-3}$	$3.5630 \cdot 10^{-3}$
1/40	$1.7425 \cdot 10^{-3}$	$1.7062 \cdot 10^{-3}$	$1.6850 \cdot 10^{-3}$	$1.6780 \cdot 10^{-3}$	$1.6757 \cdot 10^{-3}$
1/80	$8.0350 \cdot 10^{-4}$	$8.2738 \cdot 10^{-4}$	$8.1830 \cdot 10^{-4}$	$8.1523 \cdot 10^{-4}$	$8.1443 \cdot 10^{-4}$
1/160	$5.6148 \cdot 10^{-4}$	$4.0719 \cdot 10^{-4}$	$4.0342 \cdot 10^{-4}$	$4.0201 \cdot 10^{-4}$	$4.0168 \cdot 10^{-4}$

In Table 4 we compute solutions at a fixed t as before, but for a fixed Δt we compute the error of the solution computed with Δx minus the solution computed with $\Delta x/2$ and so on. We do this for several values of Δt. In this case halving Δx approximately divides the error by three.

In both tables we have taken $\alpha = 1/3$, $\tau = 1$, $R = L = 100$ and $t = 100$ with initial condition (19) for $\phi_- = 1$ and $\phi_+ = 0$.

Table 4. For a fixed value of Δt we compute the numerical solution at $t = 1000$ on $[-100, 100]$ for different values of Δx. Let $u_{\Delta t}(\Delta x, t = 100)$ denote such numerical solution. Then, in every column the table shows the error $\|u_{\Delta t}(\Delta x, t = 100) - u_{\Delta t}(\Delta x/2, t = 100))\|_\infty$ (this is the discrete L^∞-norm in x, so the difference is taken over the points of the least fine grid).

Δx	$\Delta t = 1/10$	$\Delta t = 1/20$	$\Delta t = 1/40$	$\Delta t = 1/80$	$\Delta t = 1/160$
1	$3.7060 \cdot 10^{-3}$	$3.1192 \cdot 10^{-3}$	$2.8484 \cdot 10^{-3}$	$2.7508 \cdot 10^{-3}$	$2.6230 \cdot 10^{-3}$
1/2	$1.3301 \cdot 10^{-3}$	$9.3629 \cdot 10^{-4}$	$8.3110 \cdot 10^{-4}$	$7.8267 \cdot 10^{-4}$	$7.5927 \cdot 10^{-4}$
1/4	$4.2608 \cdot 10^{-4}$	$2.9532 \cdot 10^{-4}$	$2.6003 \cdot 10^{-4}$	$2.4501 \cdot 10^{-4}$	$2.3797 \cdot 10^{-4}$
1/8	$1.3302 \cdot 10^{-4}$	$9.2615 \cdot 10^{-5}$	$8.1382 \cdot 10^{-5}$	$7.6927 \cdot 10^{-5}$	$7.4976 \cdot 10^{-5}$

5. Numerical results.

5.1. *Simulations of the travelling wave equation.*

We start by showing numerical computations of the integro-differential equation (4). For definiteness we choose $\phi_- = 1$ and $c = 1$, so that

$$h(\phi) = \phi^2 - \phi$$

and thus we expect $\phi_+ = 0$, i.e. that $\lim_{\xi\to\infty} \phi(\xi) = 0$. We impose the following initial condition:

$$\phi(\xi_0) = -1 + e^{\lambda\xi_0}$$

where λ is obtained numerically by solving (12). In order to ensure that this datum is close enough to 1, but not too close so that the solution is different from the constant solution 1, we take the truncation value ξ_0 so that

$$e^{\lambda\xi_0} \leq 10^{-4} \tag{22}$$

is satisfied. We take $\xi_0 = -1$ as the initial guess, then if with this choice the result does not satisfy (22), we double the value of ξ_0, and so on. We recall that, for large values of τ, the asymptotic behaviour (13) implies that a ξ_0 will be the more negative the larger the value of τ. In all the examples that follow we take $\Delta x = 0.01$ and we integrate the equation up to $\xi = 1000$.

Figure 1 shows results with $\alpha = 2/3$ for $\tau = 10$, where we take $\xi_0 = -100$. Figure 1(a) shows the travelling wave solution. This solution is oscillatory, but in the tail the oscillations get damped as the algebraic decay dominates the exponential oscillatory behaviour. Figure 1(b) shows a log-log plot for of the solution for $\xi \geq 550$, where we apply a linear fitting. This shows that indeed the numerical solution decays algebraically like $\phi \sim \xi^{-\alpha}$, since in this case $\alpha \approx 0.667$.

DOI: 10.1685/journal.caim.533

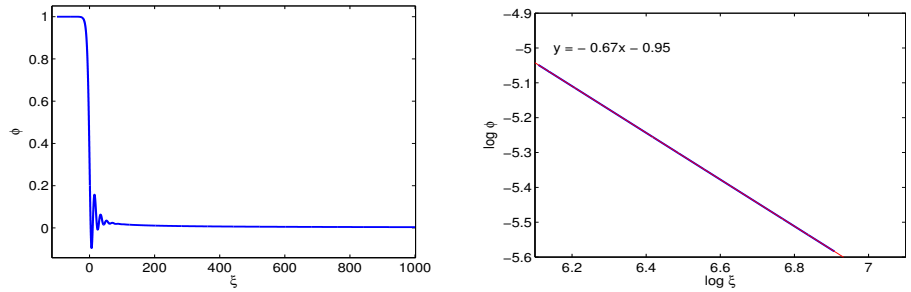

(a) ϕ against ξ. (b) $\log \phi$ against $\log \xi$.

Figure 1. Travelling wave profile for $\alpha = 2/3$ and $\tau = 10$ computed from $\xi_0 = -100$.

In Figure 2 we give too further examples with $\alpha = 2/3$. In Figure 2(a) we show the travelling wave profile for $\tau = 0.1$. In this case, with $\lambda \approx 0.885$, $\xi_0 = -16$ suffices to get the program started away from the constant solution $\phi \equiv 1$. In Figure 2(b) we show the travelling wave profiles for $\tau = 100$, which is oscillatory, and, in this case $\lambda \approx 0.0894$ and $\xi_0 = -128$ (as computed by the criterion above).

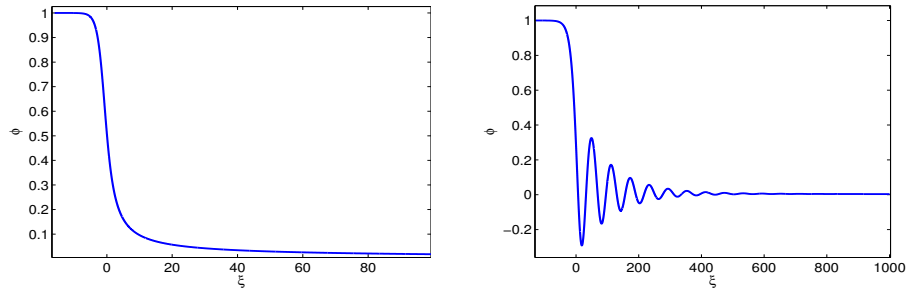

(a) Profile with $\tau = 0.1$, computed from $\xi_0 = -16$.

(b) Profile with $\tau = 100$, computed from $\xi_0 = -128$.

Figure 2. Travelling wave profile for $\alpha = 2/3$ with different values of τ.

Figure 3 shows the results $\tau = 1$ and $\alpha = 1/3 < 1/2$. In this case the program starts at $\xi_0 = -32$, here $\lambda \approx 0.4711$. Figure 1(a) shows the travelling wave solution. This solution is monotone. We observe that its decay in the tail is much slower that in the previous examples. Figure 1(b) shows a log-log plot for of the solution for $\xi \geq 550$, where we again apply a linear fitting. This shows that this numerical solution decays algebraically like $\phi \sim \xi^{-0.34}$ (here $\alpha \approx 0.334$).

In Figure 4 we give too further examples with $\alpha = 1/3$. In Figure 4(a)

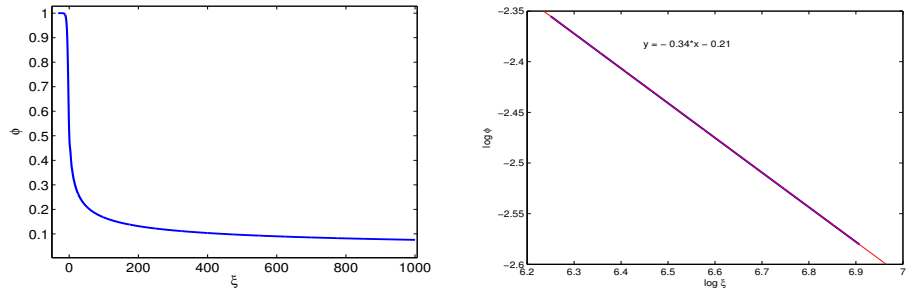

(a) ϕ against ξ. (b) $\log\phi$ against $\log\xi$.

Figure 3. Travelling wave profile for $\alpha = 1/3$ and $\tau = 1$ computed from $\xi_0 = -32$.

we show the travelling wave profile for $\tau = 0.1$. In this case, $\xi_0 = -16$, as above. In Figure 4(b) we show the travelling wave profiles for $\tau = 100$, which is oscillatory, and, in this case, the program also starts at $\xi_0 = -128$ (here we obtain that $\lambda \sim 0.814$).

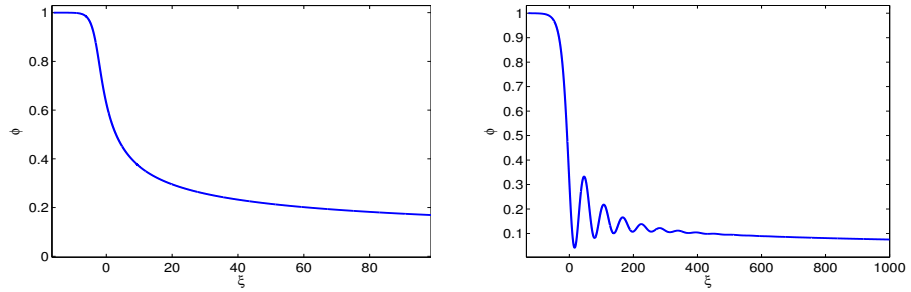

(a) Profile with $\tau = 0.1$, computed from $\xi_0 = -16$. (b) Profile with $\tau = 100$, computed from $\xi_0 = -128$.

Figure 4. Travelling wave profile for $\alpha = 1/3$ with difference values of τ.

Finally, in Figure 5 we show two examples where the travelling wave profiles are non-monotone, but they are decreasing in the tails. The values of τ for which this can occur are neither too large nor too small. Namely, for $\alpha = 2/3$ we obtain such a profile with $\tau = 2$ (see Figure 5(a)), whereas for $\alpha = 1/3$ we obtain such profile with $\tau = 4$ (see Figure 5(b)).

5.2. *Simulations of the evolution equation.*

We present results for the examples of the parameters chosen in the previous section. In particular, since we have chosen $\phi_- = 1$ and $\phi_+ = 0$, we take an initial condition $u_0(x)$ that has these far-field values. Namely

DOI: 10.1685/journal.caim.533

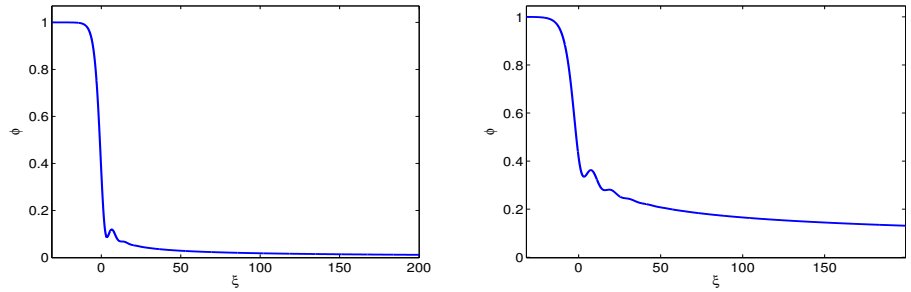

(a) Travelling wave for $\alpha = 2/3$ and $\tau = 2$.

(b) Travelling wave for $\alpha = 1/3$ and $\tau = 4$.

Figure 5. Examples showing oscillatory travelling waves, but that are decreasing in the tails.

we take

$$u_0(x) = \frac{1}{2}(1 - \tanh(\lambda(x + 80)) + \frac{1}{2(x^2 + 1)^{\alpha/2}}(1 - \tanh(-x - 80))) .$$

This initial condition decays in the tails at the same rate as travelling wave solutions, i.e. $u_0(x) = 1 + O(e^{\lambda x})$ as $x \to -\infty$ and $u_0(x) = O(1/x^{\alpha})$ as $x \to \infty$. In the examples that follow have $\Delta x = 0.25$ and $\Delta t = 0.1$. The truncated spatial domain is $[-100, 1000]$.

In Figure 6 we show an example with $\alpha = 2/3$ and $\tau = 10$. Figure 6(a) shows the profiles in space of the solution at times $t = 180$, 240 and 300. These shows how the solution has reached an oscillatory profile that moves with apparent constant speed. Figure 6(b) shows the solution profiles at times $t = 162$, 294 and 300 against the travelling wave variable $x - ct$ with $c = 1$. At $t = 162$ the solution is far from a travelling wave profile, whereas at $t = 294$ and $t = 300$ the solution behaves like one (these two profiles overlapping in this coordinate). Finally, in Figure 6(c) we show a log-log plot of the tail of the profile at time $t = 300$. This shows the the solution decays algebraically like $1/x^l$ with $l \approx 0.738$ which is a good approximation of the expected one (i.e. $\alpha \approx 0.667$, according to (16)).

In Figure 7 we show an example with $\alpha = 1/3$ and $\tau = 1$. Figure 7(a) shows the profiles in space of the solution at times $t = 180$, 240 and 300. Again, the solution at these time steps has reached a profile that moves with apparent constant speed. Figure 7(b) shows the solution profiles at times $t = 162$, 294 and 300 against the travelling wave variable $x - ct$ with $c = 1$. Again, at $t = 162$ the solution is far from a travelling wave profile, whereas at $t = 294$ and $t = 300$ the solution resembles one (these two profiles overlap in the moving coordinate). As before, we show a log-log

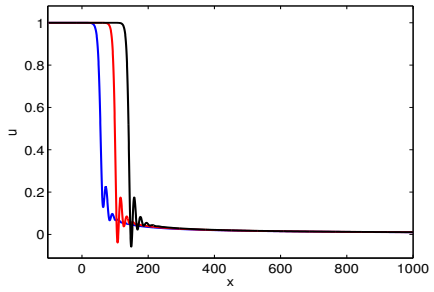

(a) Solutions against x.

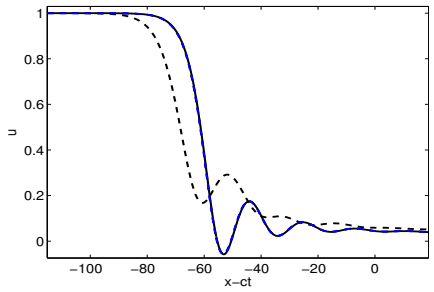

(b) Solutions against $x - ct$ with $c = 1$.

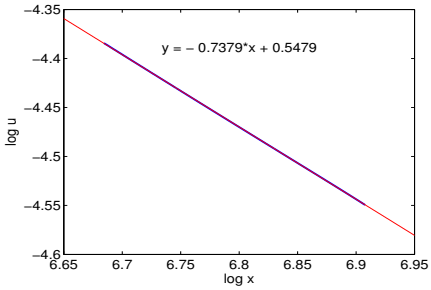

(c) Algebraic decay of the tail.

Figure 6. Results for $\alpha = 2/3$ with $\tau = 10$. (a) shows solution profiles at $t = 180$ (solid blue), $t = 240$ (solid red) and $t = 300$ (solid black) (b) shows solution profiles against $x - ct$ with $c = 1$ at $t = 162$ (dashed black), $t = 294$ (solid black) and $t = 300$ (dashed blue). (c) shows a log-log plot of the solution profile at $t = 300$.

plot of the tail of the profile, this appears in Figure 7(c) for $t = 300$. This shows that the solution decays algebraically like $1/x^l$ with $l \approx 0.384$ which is a good approximation of the expected one (i.e. $\alpha \approx 0.334$).

In order to give an illustration of the behaviour of solutions for large values of τ, we end the section by showing profiles for $\tau = 100$. Namely, Figure 8 shows profiles for $\alpha = 2/3$. Solutions for large times are shown in Figure 8(a). The same profiles nearly overlap when shown against the travelling wave variable $x - ct$ in Figure 8(b).

DOI: 10.1685/journal.caim.533

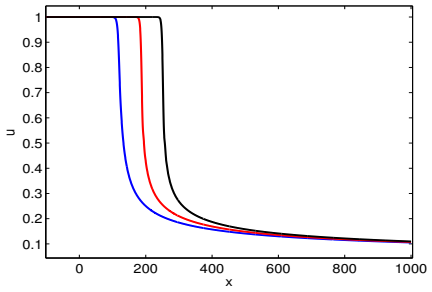

(a) Solutions against x.

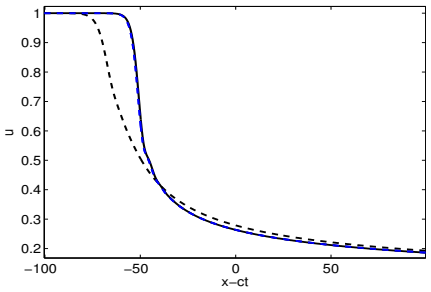

(b) Solutions against $x - ct$ with $c = 1$.

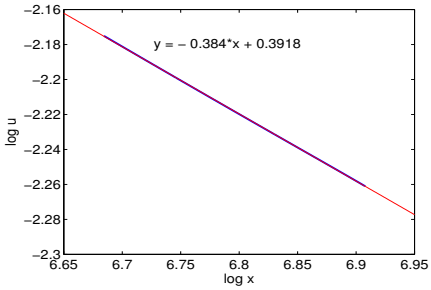

(c) Algebraic decay of the tail.

Figure 7. Results for $\alpha = 1/3$ with $\tau = 1$. (a) shows solution profiles at $t = 180$ (solid blue), $t = 240$ (solid red) and $t = 300$ (solid black) (b) shows solution profiles against $x - ct$ with $c = 1$ at $t = 162$ (dashed black), $t = 294$ (solid black) and $t = 300$ (dashed blue). (c) shows a log-log plot of the solution profile at $t = 300$.

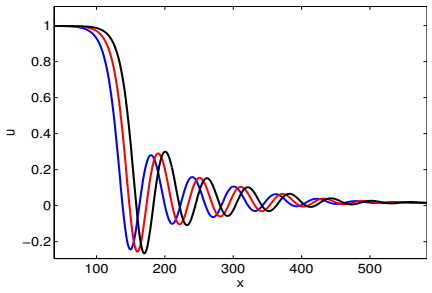

(a) Solutions against x.

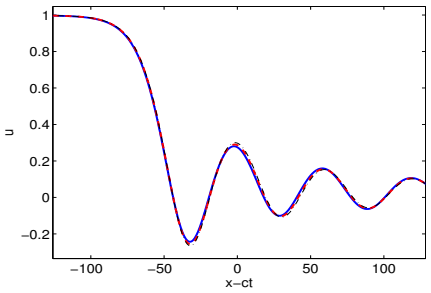

(b) Solutions against $x - ct$.

Figure 8. Results for $\alpha = 1/3$ with $\tau = 100$. (a) shows solution profiles at $t = 270$ (solid blue), $t = 285$ (solid red) and $t = 300$ (solid black). In (b) the same solution profiles are depicted against $x - ct$ with $c = 1$ ($t = 270$ with solid blue line, $t = 285$ with dashed red line and $t = 300$ with thin solid black line).

Acknowledgements.

The author wishes to thank Francisco de la Hoz for his useful suggestions on the numerical code.

REFERENCES

1. F. Achleitner, C. M. Cuesta, and S. Hittmeir, Travelling waves for a non-local Korteweg-de Vries-Burgers equation, *Journal of Differential Equations*, vol. 257, no. 3, pp. 720–758, 2014.
2. A. A. Kilbas, H. M. Srivastava, and J. J. Trujillo, *Theory and Applications of Fractional Differential Equations*, vol. 204 of *Mathematical Studies*. Elsevier, 2006.
3. F. Achleitner, S. Hittmeir, and C. Schmeiser, On nonlinear conservation laws with a nonlocal diffusion term, *Journal of Differential Equations*, vol. 250, no. 4, pp. 2177–2196, 2011.
4. A. Kluwick, E. A. Cox, A. Exner, and C. Grinschgl, On the internal structure of weakly nonlinear bores in laminar high Reynolds number flow., *Acta Mechanica*, vol. 210, pp. 135–157, 2010.
5. N. Viertl, *Viscous regularisation of weak laminar hydraulic jumps and bores in two layer shallow water flow*. PhD thesis, Technische Universität Wien, 2005.
6. W. Chester, Resonant oscillations in closed tubes, *Journal of Fluid Mechanics*, vol. 18, pp. 44–64, 1964.
7. J. Keller, Propagation of simple non-linear waves in gas-filled tubes with friction, *Zeitschrift für angewandte Mathematik und Physik*, vol. 32, pp. 170–181, 1981.
8. N. Sugimoto, Generalized Burgers equations and fractional calculus, *Nonlinear Wave Motion (ed. A. Jeffrey). Longman Scientific & Technical*, 1989.
9. N. Sugimoto, Evolution of nonlinear acoustic waves in a gas-filled pipe, in *Frontiers of Nonlinear Acoustics, 12th Intl Symp. on Nonlinear Acoustics (ed. M. F. Hamilton & D. T. Blackstock)* (E. A. Sciences, ed.), pp. 345–350, 1990.
10. N. Sugimoto, Burgers equation with a fractional derivative: hereditary effects on nonlinear acoustic waves, *Journal of Fluid Mechanics*, vol. 225, pp. 631–653, 1991.
11. J. Smoller, *Shock waves and reaction-diffusion equations*. New York: Springer, 1983.
12. A. Kluwick, S. Scheichl, and E. A. Cox, Near-critical hydraulic flows in two-layer fluids, *Journal of Fluid Mechanics*, 2007.
13. A. P. Rothmayer and F. T. Smith, *Incompressible triple-deck theory*,

DOI: 10.1685/journal.caim.533

ch. 23. CRC Press, 1998.

14. L. Prandtl, Über Flüssigkeitsbewegungen bei sehr kleiner Reibung, *Verhandlungen des III. Int. Mathem. Kongress, Teubner*, pp. 484–491, 1905.
15. J. Bona and M. Schonbek, Travelling-wave solutions of the Korteweg-de Vries-Burgers equations, *Proceedings of the Royal Society of Edinburgh A*, 1985.
16. R. Gorenflo and F. Mainardi, Fractional calculus: integral and differential equations of fractional order, in *Fractals and fractional calculus in continuum mechanics (Udine, 1996)*, vol. 378 of *CISM Courses and Lectures*, pp. 223–276, Vienna: Springer, 1997.
17. M. Schonbek, Convergence of solutions to nonlinear dispersion equations, *Communications in Partial Differential Equations*, vol. 7, pp. 959–1000, 1982.
18. U. M. Ascher and L. R. Petzold, *Computer Methods for Ordinary Differential Equations and Differential-Algebraic Equations*. Philadelphia: Society for Industrial and Applied Mathematics, 1998.
19. C. Lubich, Runge-Kutta theory for Volterra and Abel integral equations of the second kind, *Math. Comp.*, vol. 41, no. 163, p. 87102, 1983.
20. D. Richtmeyer and K. Morton, *Difference Methods for Initial Value Problems*. Wiley, New York., 1967.
21. R. Penrose, A generalized inverse for matrices, *Proceedings of the Cambridge Philosophical Society*, vol. 51, pp. 406–413, 1955.